Article

Impact of Low-intensity Pulsed Ultrasound on Transcript and Metabolite Abundance in Saccharomyces cerevisiae

Michael C. Schultz, Jian Zhang, Xian Luo, Oleksandra Savchenko, Liang Li, Michael Deyholos, and Jie Chen

J. Proteome Res., **Just Accepted Manuscript** • DOI: 10.1021/acs.jproteome.7b00273 • Publication Date (Web): 15 Jun 2017

Impact of Low-intensity Pulsed Ultrasound on Transcript and Metabolite Abundance in *Saccharomyces cerevisiae*

Michael C. Schultz[1], Jian Zhang[2,5], Xian Luo[3], Oleksandra Savchenko[4], Liang Li[3], Michael Deyholos[5] and Jie Chen* [4,6]

[1] Department of Biochemistry, University of Alberta, Edmonton, Canada

[2] InnTech Alberta, Vegreville, Alberta, Canada

[3] Department of Chemistry, University of Alberta, Edmonton, Canada

[4] Department of Biomedical Engineering, University of Alberta, Edmonton, Canada

[5] Department of Biology, University of British Columbia, Okanagan Campus, Kelowna, Canada

[6] Department of Electrical and Computer Engineering, University of Alberta, Edmonton, Canada

Corresponding Author:

Jie Chen

Tel: 1-780-492-9820

Fax: 1-780-492-1811

Email: jc65@ualberta.ca

Abstract

The interactions of ultrasound with biological materials are exploited for diagnostic, interventional and therapeutic applications in humans and can improve productivity in industrial-scale generation of organic molecules such as biofuels, vaccines and antibodies. Accordingly, there is great interest in better understanding the biological effects of ultrasound. In this paper, we studied the impact of low-intensity pulsed ultrasound (LIPUS) on RNA expression and metabolism of *S. cerevisiae*. Although the transcript expression signature of LIPUS-treated cells does not differ significantly from that of untreated cells after five days, metabolomic profiling by chemical isotopic labeling liquid chromatography mass spectrometry (CIL-LC-MS) suggests that LIPUS has an impact on the pathways of pyrimidine, proline, alanine, aspartate, glutamate and arginine metabolism. Therefore, LIPUS triggers metabolic effects beyond reprogramming of the core pathways of carbon metabolism. Further characterization of metabolism will likely be important for elucidation of the biological effects of LIPUS.

Keywords: Low-intensity pulsed ultrasound, transcriptomics, metabolomics, *Saccharomyces cerevisiae*

Introduction

Ultrasound has a frequency greater than 20 kHz (above the normal hearing range).[1, 2] By inducing the formation and collapse of microscale gas bubbles, ultrasound can generate an environment in which macromolecules are subjected to high hydrodynamic shear stress and temperature.[3, 4] The effects of these physical forces on biological materials and cells are highly variable and dependent on the type of cell, the irradiation protocol and environmental context. At the tissue level, the ultrasound methods in medical imaging are known to cause little overt damage,[5] and low-intensity pulsed ultrasound (LIPUS) can in fact promote tissue repair by stimulating the proliferation of hematopoietic stem cells as well as fibroblasts and osteoblasts.[6, 7-10] Tissue metabolism may also be altered by ultrasound as a result of microbubble collapse; the latter can induce microstreaming and microjets which may change the flow of nutrients to and from cells.[11] At the molecular level, ultrasound can affect cells by stimulating mass transfer which in turn increases the efficiency of cellular enzyme reactions including those involved in expression of proteins and other molecules (e.g., lipids in algae).[4, 12,13]

Because the biological applications of ultrasound extend from medicine to biotechnological production in microorganisms, there is intense interest in deeper understanding of the cellular responses to ultrasound. Such responses have been assessed at the population level (for example cell proliferation), and at the molecular level by application of such methods as mRNA expression profiling[14, 15] and analysis of protein post-translational modification.[16] One powerful tool for studying cell physiology, global analysis of metabolite abundance, has been little used in work on cellular effects of ultrasound. Here, we address this experimental shortfall by characterizing the metabolome of a model eukaryote, the budding yeast *Saccharomyces cerevisiae*, as it

converts glucose to the biofuel ethanol. The ultrasound treatment during this fermentation was a proprietary LIPUS treatment (frequency 1.5 MHz, duty cycle 20%) that has been previously reported to improve ethanol production by two microorganisms during fermentation.[17,18] The metabolome of control and LIPUS-treated cells was characterized by chemical isotopic labeling liquid chromatography mass spectrometry (CIL-LC-MS).[19] Metabolomic profiling was complemented by parallel global transcript profiling using RNA-seq. Our work shows that metabolic reprogramming is clearly revealed by CIL-LC-MS though cells do not exhibit a strong transcriptomic signature having undergone LIPUS treatment.

Materials and Methods

In our previous study and the current work, we used *Saccharomyces cerevisiae* strain SSL3 (spent sulfite liquor fermentation strain 3), one of the most stress tolerant strains for glucose fermentation.[20] This strain was purchased from the American Type Culture Collection (ATCC 96581). Single colonies of SSL3 for growth in liquid medium were obtained from plates incubated at 30°C for 48 hours on mYPD agar (0.3% yeast extract; 0.5% proteose peptone; 0.1% glucose; 2% agar). The designation 'mYPD' is given to highlight the fact that this YPD formulation is nutrient-poor compared to the standard in yeast molecular biology (YPD, which is 1% yeast extract; 1% bactopeptone; 2% glucose).

Inoculum preparation: One or two colonies were inoculated into 100 mL of mYPD and incubated at 180 rpm in a rotary shaker for 24 hours at 30°C. Cells were harvested by centrifugation for 5 minutes at 3000 rpm, washed with 0.9% NaCl, and then resuspended in 10 mL of medium with low yeast extract and high glucose (mYD; 0.1% yeast extract, 15% glucose, 0.5g/L $(NH_4)_2HPO_4$, 1.38 g/L NaH_2PO_4, 0.03 g/L $MgSO_4.7H_2O$ - adjusted

to pH 5.5 with 2 M NaOH before sterilization). One mL of this cell concentrate was inoculated into 100 mL mYD for the fermentation culture.

The 100 mL fermentations were carried out in 250 mL Erlenmeyer culture flasks at 30°C for 5 days in a rotary shaker as above. LIPUS (1.5 MHz, 20% duty cycle) was applied to the culture by placing each culture flask in its own water bath chamber equipped with an ultrasound transducer. Ultrasound treatments of 5 minutes each were given 12 times/day (in short, 5 minute treatments every 2 hours for the 5-day fermentation). This protocol was selected based on the previous results for *S. cerevisiae.*[18] Ultrasound was applied at 80 or 100 mW/cm^2; these conditions are referred to as 80 mW/cm^2 and 100 mW/cm^2 respectively. The control fermentations (CON) did not receive LIPUS treatment. The control and LIPUS-treated flasks were sampled for transcriptomic and metabolomic analysis at a single time point, specifically the 5-day end-point of the experiment.

This endpoint was chosen because cell number increased during the first 5 days of fermentation and then started to drop off (data not shown). A possible reason for declining activity after 5 days is that the exposure to ethanol in the closed bioreactor began to exceed the level that is readily tolerated by the strain used.[21]

Transcript Analysis

RNA was extracted from triplicate yeast cultures under CON, 80 mW/cm^2 and 100 mW/cm^2 conditions using a Qiagen RNA plant mini kit (RNeasy Plant Mini Kit, 74904). The highly purified total RNA was made into a TrueSeq Paired End 100 bp library and sequenced on an Illumina HighSeq 2000 system. The sequencing data was mapped to the Ensemble *S. cerevisiae* genome

(http://uswest.ensembl.org/Saccharomyces_cerevisiae/Info/Index) annotated with genes and transcripts using CLC Genomics Workbench 7.0.3. The number of reads per sample averaged to just under 10 million, which resulted in a mapping average of 85% of the 7126 annotated gene transcripts in the *S. cerevisiae* genome (Table S1 in Supporting Information).

Statistical analysis: ANOVA was used to identify expression differences within the entire dataset at $p<0.05$. This data subset was further analyzed as follows. Principle component and cluster analyses were performed following the procedures in the tutorial of RNA-Seq analysis (http://www.clcbio.com/wp-content/uploads/2012/08/RNA-Seq_analysis_part_I.pdf), as well as a series of t-tests comparing all three groups of samples. Fold-differences in the original normalized comparisons were used in ReVigo (http://revigo.irb.hr/) to generate gene ontology (GO) annotation enrichment profiles. These profiles were not informative because of the low overall effect of LIPUS on end-point RNA expression (see Results).

Metabolomic Profiling

Chemicals and reagents: LC-MS grade solvent (acetonitrile, methanol and water) was purchased from Thermo Fisher Scientific Canada. Glass beads (0.5 mm diameter) were purchased from Biospec Products. ^{13}C-dansyl chloride was synthesized in our lab using the protocol published previously.[19] All the other reagents and chemicals were purchased from Sigma-Aldrich Canada.

Cell lysis and metabolite extraction[22]*:* 100 μL of 50% MeOH and 0.5 mL of glass beads were added to yeast pellets in a 1.5 mL microcentrifuge tube. Five-rounds of bead

beating (one minute/round) were performed for cell lysis. After lysis, 800 μL of 50% MeOH was added for metabolite extraction. Cell debris was removed by centrifugation at 16000 x *g* at 4°C for 10 min, and the supernatant was transferred to another microcentrifuge tube and dried down in a Speed Vac (Savant SC110A). The dried extract was re-dissolved in LC-MS grade water and stored at -80°C.

Dansylation labeling: 25 μL of the metabolite extract was mixed with 12.5 μL of acetonitrile (ACN) and 12.5 μL of sodium carbonate-sodium bicarbonate buffer. The solution was then mixed with 25 μL of 18 mg/mL ^{12}C-dansyl chloride in ACN for light labeling, or 18 mg/mL ^{13}C-dansyl chloride solution in ACN for heavy labeling. The reaction was carried out at 40°C for 1 hr. After 1 hr, the reaction was cooled in an ice-water bath and 5 μL of 250 mM NaOH was added to quench the excess dansyl chloride. The solution was then incubated at 40°C for another 10 min. Finally, 25 μL of 425 mM formic acid in 1:1 ACN:H_2O (v/v) was added to consume excess NaOH and to acidify the solution.

Sample Normalization: A sample normalization step was performed before LC-MS analysis.[23] The total concentration of labeled metabolites was quantified by LC-UV in order to use the same amount of each sample for metabolome comparison. 2 μL of the labeled solution was injected onto a Phenomenex Kinetex C18 column (2.1 mm × 5 cm, 1.7 μm particle size, 100 Å pore size) linked to a Waters ACQUITY UPLC system (Waters, Milford, MA) for step-gradient LC-UV. Mobile phase A was 5% (v/v) ACN in water with 0.1% (v/v) formic acid added, and mobile phase B was acetonitrile with 0.1% (v/v) formic acid added. The step-gradient used for LC-UV was: t=0 min, 100% A; t=1

min, 100% A; t=1.1 min, 5% A; t=2.5 min, 5% A; t=3min, 100% A; t=6 min, 100% A. The flow rate was 450 μL/min. The UV detector was operated at 338 nm.

LC-MS: The ^{12}C-/^{13}C-mixtures were injected onto a Dionex Ultimate 3000 UHPLC system (Thermo Fisher Scientific) linked to a Bruker Maxis Impact Quadrupole Time-of-flight (Q-TOF) mass spectrometer (Bruker, Billerica, MA). Separations were performed on an Agilent reversed phase Eclipse Plus C18 column (2.1 mm × 10 cm, 1.8 μm particle size, 95 Å pore size). Mobile phase A was 5% (v/v) ACN in water with 0.1% (v/v) formic acid, and mobile phase B was acetonitrile with 0.1% (v/v) formic acid. The chromatographic conditions were: t = 0 min, 20% B; t = 3.5 min, 35% B; t = 18 min, 65% B; t = 21 min, 95% B; t = 26 min, 95%; t=34 min, 95% B. The flow rate was 180 μL/min. The mass spectrometer conditions were as follows: capillary voltage, 4500 V; end plate offset, 500V; dry temperature, 230°C; spectra rate, 1.0 Hz; nebulizer, 1.0 bar; dry gas, 8 L/min. All MS spectra were obtained in the positive ion mode.

Data Processing and Analysis: The raw data was exported as a .csv file, which included m/z, peak intensity, peak width and retention time. Peak pairs extraction, peak filter and peak ratio calculations were conducted using the software tool IsoMS.[24] The files were aligned by each feature's retention time and accurate mass. The missing values in features were filled in using a Zerofill script.[25] Principal component analysis (PCA), partial least squares discriminant analysis (PLS-DA), and pathway enrichment analysis were all performed using the website-based statistical tool MetaboAnalyst (www.metaboanalyst.ca).[26] Volcano plots were generated by Origin 2015. Metabolite positive identification was done based on retention time and accurate mass match to a DnsID library (www.mycompoundid.org).[27] Metabolite putative identification was

performed based on accurate mass match to the metabolites in the human metabolome database (HMDB) (www.hmdb.ca)[28] and the evidence-based metabolome library in MyCompoundID (MCID) (www.mycompoundid.org)[29] with one reaction. The MCID library is composed of 8,021 known human endogenous metabolites and 375,809 predicted metabolites from one metabolic reaction.

Results

This initial exploration of global molecular effects of LIPUS on *S. cerevisiae* is an end-point study of steady state RNA and metabolite abundance.

Analysis of Annotated Transcripts

Data obtained by RNA-seq of total RNA were used to compare the expression level of annotated transcripts in control and LIPUS-treated cells. ANOVA without a fold-change threshold filer revealed that 354 annotated transcripts showed a significant difference in expression (reads) between the three groups of samples (Table S2 in Supporting Information). Consistent with an effect of LIPUS on transcript abundance, PCA of the log transformed expression data separated the 100 mW/cm^2 sample set from CON and 80 mW/cm^2 (Figure 1). CON and 80 mW/cm^2, on the other hand, were not widely separated. While global statistical analysis did not separate both 80 mW/cm^2 and 100 mW/cm^2 from CON, the data for the treatment groups does hint at an effect of LIPUS on RNA expression levels. Specifically, considering differences that satisfy the $p \leq 0.05$ threshold, the 80 mW/cm^2 and 100 mW/cm^2 groups share 23 genomic features that correspond to transcripts that differ in abundance from the CON samples (Table 1).

The analyses in Figure 1 and Table S2 in Supporting Information were refined by filtering to include only those mRNA expression differences that likely affect protein synthesis in the cell, that is, expression differences higher than 2-fold.[30,31] When this filter is applied to the data, it is evident that neither 80 mW/cm^2 nor 100 mW/cm^2 differs substantially from CON (Table S3 in Supporting Information). That is, only YML039W (retrotransposon TYA Gag and TYB Pol genes) differs between 80 mW/cm^2 and CON (-2.6 fold), and only *YPT6*, *RIP1* and uncharacterized ORF YDL071C differ between 100 mW/cm^2 and CON (respectively 2.1, 2 and 3.6 fold). Furthermore, no mRNA that differs in abundance by 2-fold or more between 80 mW/cm^2 and CON also differs in expression between 100 mW/cm^2 and CON, and the gene that differs in expression between CON and 80 mW/cm^2 is not in the same pathway or functional category as any gene that differs between CON and 100 mW/cm^2. Since 80 mW/cm^2 and 100 mW/cm^2 have the same effect on ethanol production,[18] it follows that the molecular mechanism by which these treatments improve biofuel yield is not reflected in end-point mRNA concentration differences that could underlie population-wide differences in protein expression level.

Metabolomic Profiling

RNA-seq analysis revealed only a modest effect of LIPUS on transcript abundance. Since LIPUS causes increased cellular production of ethanol,[18] we turned out attention to the possibility that steady state levels of other intracellular metabolites differ between the control and the LIPUS-treated cells. We used metabolomics to explore this possibility. The analytical method employed was chemical isotopic labeling liquid chromatography mass spectrometry (CIL-LC-MS). Isotope labeling was achieved by dansylation, which is advantageous because it improves the sensitivity of metabolite detection, and metabolite separation by reversed phase chromatography.[19] First, each individual sample was subject

to ^{12}C-dansylation labeling. The total concentration of dansylation-labeled metabolites in each individual sample was then determined by LC-UV. Based on these measurements, equal amounts of each individual sample were mixed to generate a pooled sample, which was labeled using ^{13}C-dansyl chloride. After that, each ^{12}C-dansylation-labeled individual sample was mixed with an equal amount of the ^{13}C-dansylation-labeled pooled sample, and the ^{12}C- /^{13}C-mixture injected onto LC-MS for analysis. Metabolite identification was based on retention time and accurate mass match to appropriate libraries. The data were analyzed by statistical tools to identify the dysregulated metabolites.

In total, 4035 peak pairs or putative metabolites were detected from aligned files, which combined the CON, 80 mW/cm^2 and 100 mW/cm^2 groups. We first searched against the DnsID library, which contains 275 standards with accurate mass and retention time, for positive metabolite identification. Ninety-three metabolites have a match in the DnsID library (Table S4 in Supporting Information). Putative metabolite identification was also performed by searching accurate mass against HMDB, and 640 peak pairs were matched to metabolites (Table S5 in Supporting Information). We further searched against the predicted metabolome library MCID and identified an additional 1694 metabolite matches (Table S6 in Supporting Information). Therefore, we identified 2334 metabolites out of 4035 peak pairs for a 58% matching rate.

Multivariate PCA was performed to visualize all the metabolite information obtained in the profiling experiment (Fig. 2A). In the plot, the 80 mW/cm^2 and CON samples overlap, while the 100 mW/cm^2 samples are separated well on principal component 2 (PC 2) from other two. The PCA is an unsupervised data reduction technique, and thus the correlation

between predictive variables and target variables is not considered. As a complement to PCA, PLS-DA was also performed to examine the metabolome dataset. Figure 2B shows that there is only a slight separation between the CON and 80 mW/cm^2 samples, but a clear separation on component 1 between the 100 mW/cm^2 and CON. This indicates that LIPUS can affect the steady state abundance of intracellular metabolites in yeast. Ethanol production does not differ between 80 mW/cm^2 and 100 mW/cm^2,[18] but 100 mW/cm^2 caused metabolite alterations that were not elicited by the 80 mW/cm^2 treatment. From these observations, we consider it unlikely that the metabolite abundance differences between CON and 100 mW/cm^2 are, on their own, reflective of metabolic events that lead to higher biofuel production.

We plotted the PCA and PLS-DA of only the CON and 100 mW/cm^2 groups to further evaluate the influence of LIPUS on metabolite abundance in yeast cells. These two groups clearly separate from each other on PC1 in the PCA score plot (Fig 2C). The two groups also separate on component 1 in the PLS-DA score plot (Fig. 2D). The model that the CON and 100 mW/cm^2 groups are distinct was subjected to a cross-validation test. R^2, which estimates how well the model fits the data, is 0.99; Q^2, which describes predictive ability of the model, is 0.93.[32,33] Together these analyses confirm the robustness of the PLS-DA model.

Volcano plots of CON versus 80 mW/cm^2 (Fig. 3A) and CON versus 100 mW/cm^2 (Fig. 3B) were also used to visualize the metabolomics data. At the threshold of p=0.05, the fold change cut-off value for up-regulated and down-regulated metabolites was 1.20 and 0.83, respectively. Comparing CON and 100 mW/cm^2 there are 434 upregulated metabolites and 229 down regulated metabolites (Fig. 3B). The number of dysregulated

metabolites is lower when comparing CON and 80 mW/cm^2: there are only 87 upregulated metabolites and 36 downregulated metabolites (Fig. 3A). These results further confirm that the 100 mW/cm^2 treatment has a more significant effect on yeast metabolism than the lower dose 80 mW/cm^2 treatment.

Table 2 lists the metabolites that differ significantly in abundance between CON and 100 mW/cm^2, and have been definitively identified. Two metabolites with increased steady state abundance in the 100 mW/cm^2 treatment group, namely β-alanine and pantothenic acid, have a direct precursor-product relationship.[34,35,36] Interestingly four other dysregulated metabolites – uridine, uracil, N-acetyl-putrescine and ornithine – all potentially contribute to the synthesis of β-alanine. Considering this data in the context of the organization of yeast metabolic pathways,[37] it is plausible that LIPUS affects the metabolism of pyrimidine and five amino acids (proline, alanine, aspartate, glutamate and arginine) (Fig. 4A). In part this conclusion is consistent with the result of an *in silico* analysis in which metabolites that differ in abundance between the three sample groups were input into the Pathway Analysis tool in Metaboanalyst. This tool combines enrichment analysis based on metabolite concentrations with pathway topology analysis, which takes into account the structure of pathways. In the diagram shown in Figure 4B, the y-axis represents the p-value calculated from pathway enrichment analysis, while x-axis represents the pathway impact values from topological analysis. The deeper red color represents a larger p-value, and a larger node radius represents a larger impact value. This pathway impact visualization reveals some of the same relationships as manual analysis. Overall the metabolomics data are consistent with an effect of LIPUS on mechanisms that tie into the pathways of pyrimidine, proline, alanine, aspartate, glutamate and arginine metabolism.

Discussion

The yield of ethanol from high-glucose cultures of *S. cerevisiae* strain SSL3 is significantly improved by LIPUS.[18] Here we explored the possibility that transcriptomic and metabolomic profiling will reveal biological mechanisms that contribute to this effect.

The current endpoint analysis of transcript abundance suggests that modulation of mRNA availability for translation is not an important mechanism of physiological reprogramming by LIPUS. This is somewhat surprizing because transcriptional and translational regulation make a major contribution to the normal control of glucose and ethanol metabolism in yeast.[33] It is possible that some effects of LIPUS on transcript abundance in cells were not detected because they occurred early during the LIPUS treatment and were transient. This scenario is not unreasonable considering that transcription can be reprogrammed during glucose depletion from the medium even when its total level remains sufficient for robust fermentative metabolism and exponential growth.[38] Future detailed time course studies in which transcript abundance is monitored in parallel with the proliferation state of cells and glucose and ethanol levels in the culture will be required to test this hypothesis.

For cells harvested at the completion of the growth phase under fermentation conditions, metabolomics was a much more effective tool than transcriptomics for revealing physiological responses to LIPUS treatment. That is, while the small number of transcript changes revealed by RNA-seq could not be mapped onto a plausible cell response pathway, the pattern of metabolite changes under LIPUS suggested that flux through

interdependent pathways of metabolism is affected by this treatment (Fig. 4A). Therefore, metabolomics analysis is a promising avenue for further characterization of how cells react to LIPUS. The time course studies proposed for transcriptomics analysis may serve as an important guide for future metabolomics experiments. In particular, if the temporal studies reveal a transient effect of LIPUS on the transcriptome, then it would likely be profitable to perform a detailed study of metabolomic reprogramming during this time interval.

Conclusion

We studied the impact of LIPUS on RNA expression and metabolism of S. cerevisiae. Metabolomic profiling by CIL-LC-MS indicated that LIPUS has an impact on the pathways of alanine, arginine, aspartate, glutamate, proline, and pyrimidine metabolism, though the transcript expression signature of LIPUS treated S. cerevisiae did not differ significantly compared to the untreated cells after five days. LIPUS activates metabolic effects beyond reprogramming of the core pathways of carbon metabolism.

Associated Content – Supporting Information tables

Table S1. Number of reads and percent genes mapped per sample.

Table S2. Pairwise comparison of all conditions by ANOVA. Statistically significant expression differences were evident for 354 genes.

Table S3. mRNA expression differences filtered by p value.

Table S4. Metabolites identified by searching against DnsID.

Table S5. Putative metabolite identification was performed by searching accurate mass against HMDB, and 640 peak pairs were matched to metabolites.

Table S6. The predicted metabolome library MCID was searched, and an additional 1694 metabolite matches were identified.

Acknowledgements

The co-authors would like to thank the funding support from the Natural Sciences and Engineering Research Council of Canada & Alberta Innovates Technology Future. We also would like to thank Susan Koziel from InnTech Alberta, Vegreville, Alberta, Canada for helping RNA studies.

Competing financial interests

The authors declare no competing financial interests.

Author Contributions

M. S. -- wrote the main manuscript text and interpreted the high-throughput data,

J. Z. -- proposed the original idea, designed and conducted the RNA studies,

X. L. – conducted the metabolic tests and drafted the metabolomics data analysis discussion,

O. S. – carried out the ultrasound experiments,

L. L. -- supervised the metabolic tests,

M. D. -- supervised and helped design the RNA studies,

J. C. – proposed the original ideas, wrote and finalized the manuscript text, monitored the research progress

References

(1) Patist, A.; Bates, D. Ultrasonic innovations in the food industry: From the laboratory to commercial production. *Innovative Food Science & Emerging Technologies* **2008**, 9:147-154.

(2) Khanal, S.K.; Montalbo, M.; van Leeuwen, J.; Srinivasan, G.; Grewell, D. Ultrasound enhanced glucose release from corn in ethanol plants. *Biotechnology and Bioengineering* **2007**, 98(5), 978-985.

(3) Pandey, A. (ed.) Handbook of plant-based biofuels. *CRC Press* **2008**, ISBN-13:978-1560221753. ISBN-10:1560221755

(4) Stathopulos, P. B.; Scholz, G. A.; Hwang, Y. M.; Rumfeldt, J.; Lepock, J. R.; Meiering, E. M. Sonication of proteins causes formation of aggregates that resemble amyloid. *Protein Sci.* **2004**, 13(11):3017-27.

(5) Nyborg, W.L. Biological effects of ultrasound: development of safety guidelines. Part II: general review. *Ultrasound Med Biol*. **2001**, 27(3):301-33.

(6) Peng Xu, Gul-Uludag, H.; Ang, W. T.; Yang, X.; Huang, M.; Marquez-Curtis, L.; McGann, L.; Janowska-Wieczorek, A.; Xing, J.; Swanson, E.; Chen, J. Low-intensity pulsed ultrasound-mediated stimulation of hematopoietic stem/progenitor cell viability, proliferation and differentiation in vitro. *Biotechnology Letters*, **2012**, 34(10):1965-1973.

(7) Doan, N.; Reher, P.; Meghji, S.; Harris, M. In vitro effects of therapeutic ultrasound on cell proliferation, protein synthesis, and cytokine production by human fibroblasts, osteoblasts, and monocytes. *J Oral Maxillofac Surg* **1999**, 57:409–419.

(8) Zhou, S.; Schmelz, A.; Seufferlein, T.; Li, Y.; Zhao, J.; Bachem, M. G. Molecular mechanism of low intensity pulsed ultrasound in human skin fibroblast. *J Biol Chem* **2004**, 279:54463-54469.

(9) Min, B.H.; Woo, J. I.; Cho, H. S.; Choi, B. H.; Park, S. J.; Choi, M. J.; Park, S. R. Effects of low-intensity ultrasound (LIUS) stimulation on human cartilage explants. *Scand J Rheumatol* **2006**, 35:305–311.

(10) Sun, J.S.; Hong, R-C.; Chang, W.; Chen, L-T.; Lin, F-H.; Liu, H-C. In vitro effects of low-intensity ultrasound stimulation on the bone cells. *J Biomed Mater Res*. 2001, 57:449-56.

(11) Ashokkumar, M. Applications of ultrasound in food and bioprocessing. *Ultrasonics Sonochemistry*. **2015**, 25(1), 17–23.

(12) Wood, B.E.; Aldrich H.C.; Ingram L.O. Ultrasound stimulates ethanol production during the simultaneous saccharification and fermentation of mixed waste office paper. *Biotechnology Progress* **1997**, 13(3), 232-237.

(13) Savchenko, O.; Xing, J.; Yang, X.; Gu, Q.; Shaheen, M.; Huang, M.; Yu, X.; Burrell, R.; Patra, P.; Chen, J. Algal cell response to pulsed waved stimulation and its application to increase algal lipid production. *Scientific Reports* **2017**, 7(42003).

(14) Martin, E. The cellular bioeffects of low intensity ultrasound. *Ultrasound* **2009,** 17: 214-219.

(15) Furusawa, Y.; Hassan, M.A.; Zhao, Q.L.; Ogawa, R.; Tabuchi, Y.; Kondo, T. Effects of therapeutic ultrasound on the nucleus and genomic DNA. *Ultrason Sonochem* **2014**, 21(6):2061-8.

(16) Shindo, T., Ito, K.; Ogata, T.; Hatanaka, K.; Kurosawa, R.; Eguchi, K.; Kagaya, Y.; Hanawa, K.; Aizawa, K.; Shiroto, T.; Kasukabe, S.; Miyata, S.; Taki, H.; Hasegawa, H.; Kanai, H.; Shimokawa, H. Low intensity pulsed ultrasound enhances angiogenesis and amelioratesLeft ventricular dysfunction in a mouse model of acute myocardial infarction. *Arterioscler Thromb Vasc Biol.* **2016**, 36(6):1220-9.

(17) Zhao, Y.P.; Ang, T.W.; Xing, J.; Zhang, J.; Chen, J. Applications of Ultrasound to

Enhance Mycophenolic Acid Production. *Ultrasound in Med. & Biol.* **2012**, 38(9):1582–1588.

(18) Shaheen, M.; Choi, M.; Ang, W.; Zhao, Y.; Xing, J.; Yang, R.; Xing, J.; Zhang, J.; Chen, J. Application of Low-Intensity Pulsed Ultrasound to Increase Bio-ethanol Production. *Renewable Energy* **2013**, 57:462-468.

(19) Guo, K.; Li, L. Differential 12C-/13C-isotope dansylation labeling and fast liquid chromatography/mass spectrometry for absolute and relative quantification of the metabolome. *Anal. Chem*. **2009**, 81:3919-3932.

(20) Linden, T.; Peetre, J.; Hahn-Hagerdal B. Isolation and characterization of acetic-tolerant galactose-fermenting strains of saccharomyces cerevisiae from a spent sulfite liquor fermentation plant. *Applied and Environmental Microbiology* **1992**, 58(5):1661-1669.

(21) Stanley, D.; Bandara, A.; Fraser, S.; Chambers, P.J.; Stanley, G.A. The ethanol stress response and ethanol tolerance of Saccharomyces cerevisiae. *J Appl Microbiol*. **2010**, 109(1):13-24.

(22) Luo, X.; Zhao, S.; Huan, T.; Sun, D.; Magnus, R.; Friis, N.; Schultz, M. C.; Li, L. High-Performance Chemical Isotope Labeling Liquid Chromatography-Mass Spectrometry for Profiling the Metabolomic Reprogramming Elicited by Ammonium Limitation in Yeast. *J Proteome Res* **2016**, 15(5):1602-12.

(23) Wu, Y. M.; Li, L. Determination of Total Concentration of Chemically Labeled Metabolites as a Means of Metabolome Sample Normalization and Sample Loading Optimization in Mass Spectrometry-Based Metabolomics. *Anal. Chem*. **2012**, 84:10723-10731.

(24) Zhou, R.; Tseng, C. L.; Huan, T.; Li, L. IsoMS: automated processing of LC-MS data generated by a chemical isotope labeling metabolomics platform. *Anal. Chem*. **2014**,

86:4675-4679.

(25) Huan T.; Li L. Counting missing values in a metabolite-intensity data set for measuring the analytical performance of a metabolomics platform. *Anal. Chem.* **2015**, 87:1306-1313.

(26) Tseng, C. L.; Li, L. High-performance isotope-labeling liquid chromatography mass spectrometry for investigating the effect of drinking Goji tea on urine metabolome profiling. *Sci. China-Chem*. **2014**, 57:678-685.

(27) Huan, T.; Wu, Y.; Tang, C.; Lin, G.; Li, L. MyCompoundID MS/MS search: metabolite identification using a library of predicted fragment-ion-spectra of 383,830 possible human metabolites. *Anal. Chem*. **2015**, 87: 9838-9845.

(28) Wishart, D.S.; Jewison, T.; Guo, A. C.; Wilson, M.; Knox, C.; Liu, Y.; Djoumbou, Y.; Mandal, R.; Aziat, F.; Dong, E.; Bouatra, S.; Sinelnikov, I.; Arndt, D.; Xia, J.; Liu, P.; Yallou, F.; Bjorndahl, T.; Perez-Pineiro, R.; Eisner, R.; Allen, F.; Neveu, V.; Greiner, R.; Scalbert, A. HMDB 3.0--the human metabolome database in 2013, *Nucleic Acids Res*. **2013**, 41:D801-D807.

(29) Li, L.; Li, R.; Zhou, J.; Zuniga, A.; Stanislaus, A. E.; Wu, Y.; Huan, T.; Zheng, J.; Shi, Y.; Wishart, D. S.; Lin, G. MyCompoundID: Using an evidence-based metabolome library for metabolite identification. *Anal. Chem*. **2013**, 85:3401-3408.

(30) Breitkreutz, A.; Boucher, L.; Breitkreutz, B-J; Sultan, M.; Jurisica, I.; Tyers, M. Phenotypic and transcriptional plasticity directed by a yeast mitogen-activated protein kinase network. *Genetics*. **2003**, 165(3):997-1015.

(31) Carvalho-Netto, O.V.; Carazzolle, M. F.; Mofatto, L. S.; Teixeira, P.; Noronha, M. F.; Calderón, L.; Mieczkowski, P.A.; Argueso, J. L.; Pereira, G. Saccharomyces cerevisiae transcriptional reprograming due to bacterial contamination during industrial scale bioethanol production, *Microb Cell Fact.* **2015**, 14:13.

(32) Xia, J.G.; Wishart, D.S. Web-based inference of biological patterns, functions and pathways from metabolomic data using MetaboAnalyst. *Nat Protoc* **2011**, 6 (6):743-760.

(33) Xu, W.; Chen, D.; Wang, N.; Zhang, T.; Zhou, R.; Huan, T.; Lu, Y.; Su, X.; Xie, Q.; Li, L.; Li, L. J. Development of high-performance chemical isotope labeling LC–MS for profiling the human fecal metabolome. *Anal Chem* **2015**, 87(2):829-836.

(34) Slavov, N.; Budnik, B. A.; Schwab, D.; Airoldi, E. M.; van Oudenaarden, A. Constant growth rate can be supported by decreasing energy flux and increasing aerobic glycolysis. *Cell Rep.* **2014**, 7(3):705-14.

(35) Snyder, N.W.; Tombline, G.; Worth, A. J.; Parry, R.C.; Silvers, J.A.; Gillespie, K.P.; Basu, S. S.; Millen, J.; Goldfarb, D.S.; Blair, I. A. Production of stable isotope-labeled acyl-coenzyme A thioesters by yeast stable isotope labeling by essential nutrients in cell culture. *Anal Biochem* **2015**, 474:59-65.

(36) White, W.H.; Gunyuzlu, P.L.; Toyn, J.H. Saccharomyces cerevisiae is capable of de Novo pantothenic acid biosynthesis involving a novel pathway of beta-alanine production from spermine. *J Biol Chem* **2001**, 276(14):10794-800.

(37) Kanehisa, M.; Sato, Y.; Kawashima, M.; Furumichi, M.; Tanabe, M. KEGG as a reference resource for gene and protein annotation. *Nucleic Acids Res.* **2016**, 44(D1):D457-62.

(38) Zaman, S.; Lippman, S.I.; Zhao, X.; Broach J.R. How saccharomyces responds to nutrients. *Annu Rev Genet*. **2008**, 42:27-81.

Table 1. Low magnitude but statistically significant transcript abundance differences between control and LIPUS-treated samples (two-tailed T test).

			CON vs 80 mW/cm^2		CON vs 100 mW/cm^2	
Systematic name	**Gene**	**Brief description**	**Fold change**	**p value**	**Fold change**	**p value**
YDL126C	*CDC48*	AAA ATPase; subunit of polyUb-selective segregase complex	-1.13	0.02	-1.19	1.53E-03
YDR099W	*BMH2*	14-3-3 protein, minor isoform	1.17	0.05	1.31	0.01
YER074W	*RPS24A*	Ribosomal 40S subunit protein S24A	-1.09	0.04	-1.1	5.15E-03
YGL067W	*NPY1*	Peroxisomal NADH diphosphatase (pyrophosphatase)	1.21	0.05	1.26	0.02
YIL009C-A	*EST3*	Component of the telomerase holoenzyme	-1.3	0.03	-1.4	0.03
YIR035C	*NRE1*	Putative cytoplasmic short-chain dehydrogenase/reductase	1.37	0.04	1.21	0.03
YJL075C		ORF, Dubious	-1.22	0.05	-1.33	0.05
YKL053W		ORF, Dubious	-1.48	5.14E-03	-1.32	0.02
YKL187C	*FAT3*	Required for fatty acid uptake; mitochondrion-associated	1.52	0.05	1.75	0.05
YLL037W		ORF, Dubious	-1.36	0.04	-1.56	0.03
YLR174W	*IDP2*	Cytosolic NADP-specific isocitrate dehydrogenase	-1.23	0.02	-1.23	0.03
YML079W		ORF , Uncharacterized	-1.19	0.02	-1.21	0.04
YMR260C	*TIF11*	Translation initiation factor eIF1A	-1.14	0.01	-1.11	0.01
YNL113W	*RPC19*	RNA polymerase subunit AC19	1.32	0.02	1.43	9.71E-03
YNL298W	*CLA4*	Cdc42p-activated protein kinase	-1.18	0.02	-1.29	8.79E-03
YNR026C	*SEC12*	Guanine nucleotide exchange factor involved in ER to Golgi transport	1.26	0.05	1.25	0.01
YNR035C	*ARC35*	Subunit of the ARP2/3 complex	-1.19	0.04	-1.2	0.04
YOL054W	*PSH1*	E3 ubiquitin ligase	1.1	0.05	1.18	0.01
YOL096C	*COQ3*	Mitochondrial O-methyltransferase	-1.14	0.05	-1.24	0.01
YOR040W	*GLO4*	Mitochondrial glyoxalase II	1.43	5.59E-03	1.59	0.04
YPL179W	*PPQ1*	PP1 family protein phosphatase	1.34	0.05	1.36	0.05
YPL274W	*SAM3*	High-affinity S-adenosylmethionine permease	-1.12	0.03	-1.25	0.05
YPR126C		ORF , Dubious	1.49	0.03	1.49	0.03

Table 2. Metabolites that differ significantly between CON and 100 mW/cm^2 and have been definitively identified.

HMDB No.	Name	Fold change	p value
HMDB00300	Uracil	0.75	0.001898
HMDB00214	Ornithine	0.73	0.007194
HMDB00279	Saccharopine	1.22	0.049021
HMDB00670	Homo-L-arginine	1.87	2.15E-06
HMDB00641	L-Glutamine	1.29	1.03E-05
HMDB00149	Ethanolamine	1.24	0.000549
HMDB02064	N-Acetylputrescine	1.30	0.007016
HMDB00056	Beta-Alanine	1.96	2.01E-06
HMDB00296	Uridine	1.35	5.35E-05
HMDB03337	Oxidized glutathione	1.20	0.031509
HMDB00210	Pantothenic acid	1.48	2.93E-05
HMDB00296_2	Uridine - H2O	1.43	0.000121
HMDB00939	S-Adenosylhomocysteine	1.33	0.007566
HMDB00759	Glycyl-L-Leucine	1.35	0.003507
HMDB28691	Alanyl-Leucine	1.34	0.004264
HMDB28848	Glycyl-Phenylalanine	1.48	0.002568
HMDB28694	Alanyl-Phenylalanine	1.28	0.024969
HMDB04987	Alpha-Aspartyl-lysine	1.44	0.002311
HMDB00440	3-Hydroxyphenylacetic acid	1.29	0.008094
HMDB28853	Glycyl-Tyrosine	1.41	0.000138

Figure 1: PCA analysis of control and LIPUS-treated samples by RNA expression values. Sample points are plotted according to PCA of the log transformed RNA-seq data that were statistically significant by ANOVA.

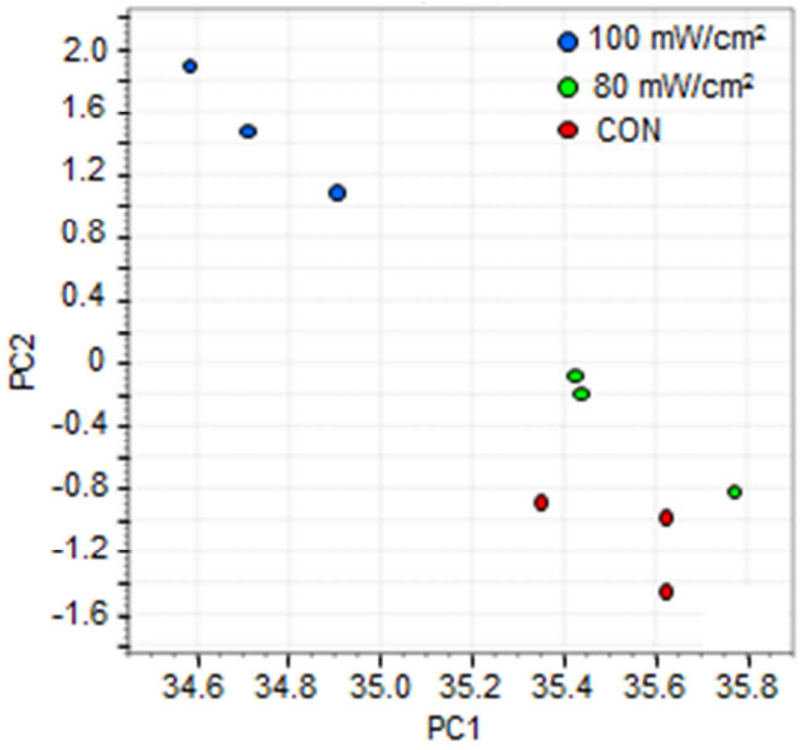

Figure 2: PCA and PLS-DA analysis of control and LIPUS-treated samples by relative metabolite abundance. (A) PCA and (B) PLS-DA scoring plots of control, 80 mW/cm^2 and 100 mW/cm^2 treated groups. (C) PCA and (D) PLS-DA scoring plots of control and 100 mW/cm^2 treated groups.

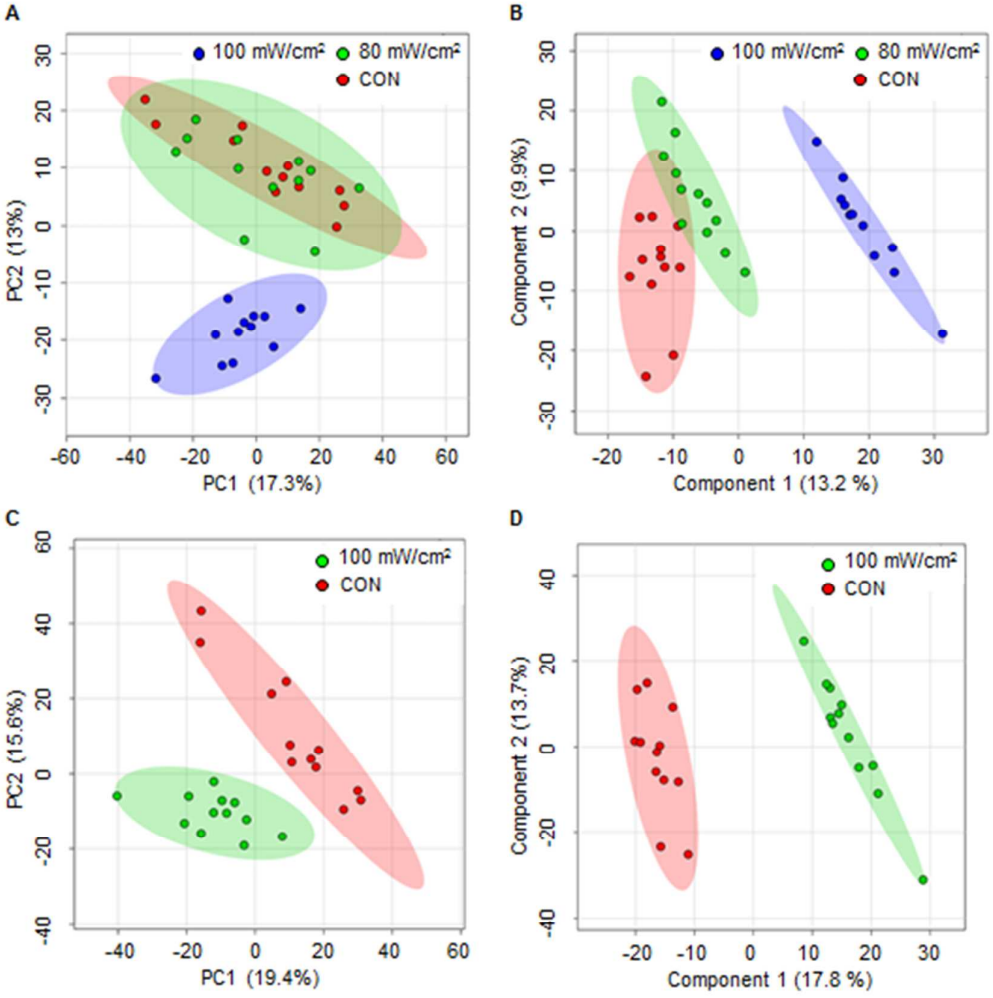

Figure 3: Volcano plots of metabolite abundance in LIPUS-treated cells relative to the control. (A) 80 mW/cm^2 versus the control. (B) 100 mW/cm^2 versus the control. The up- and down-regulated metabolites (1.2-fold threshold, $p \leqslant 0.05$) are marked in red and green, respectively.

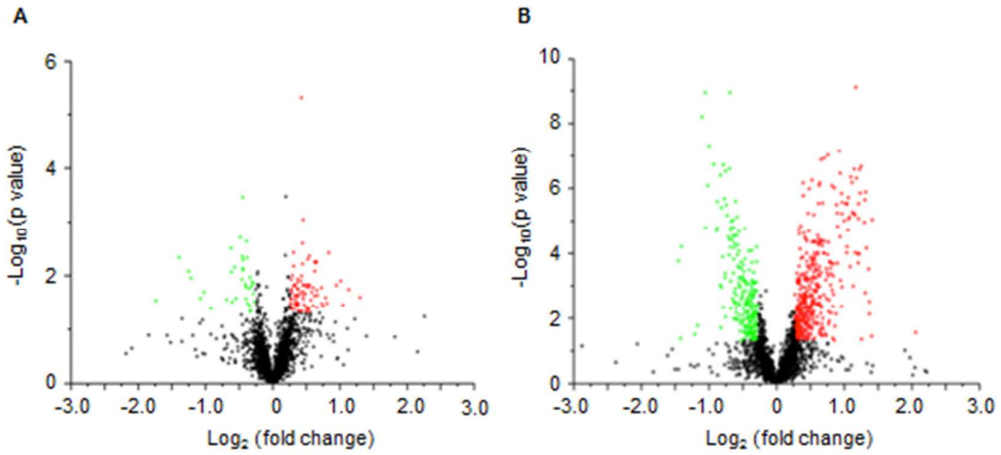

Figure 4： Metabolic pathway analysis. (A) Pathway relationships of dysregulated metabolites suggested by manual mapping of the CON versus 100 mW/cm^2 metabolite data onto the metabolic chart of yeast. (B) Overview of metabolic pathway enrichment analysis result using Pathway Analysis tools in Metaboanalyst.

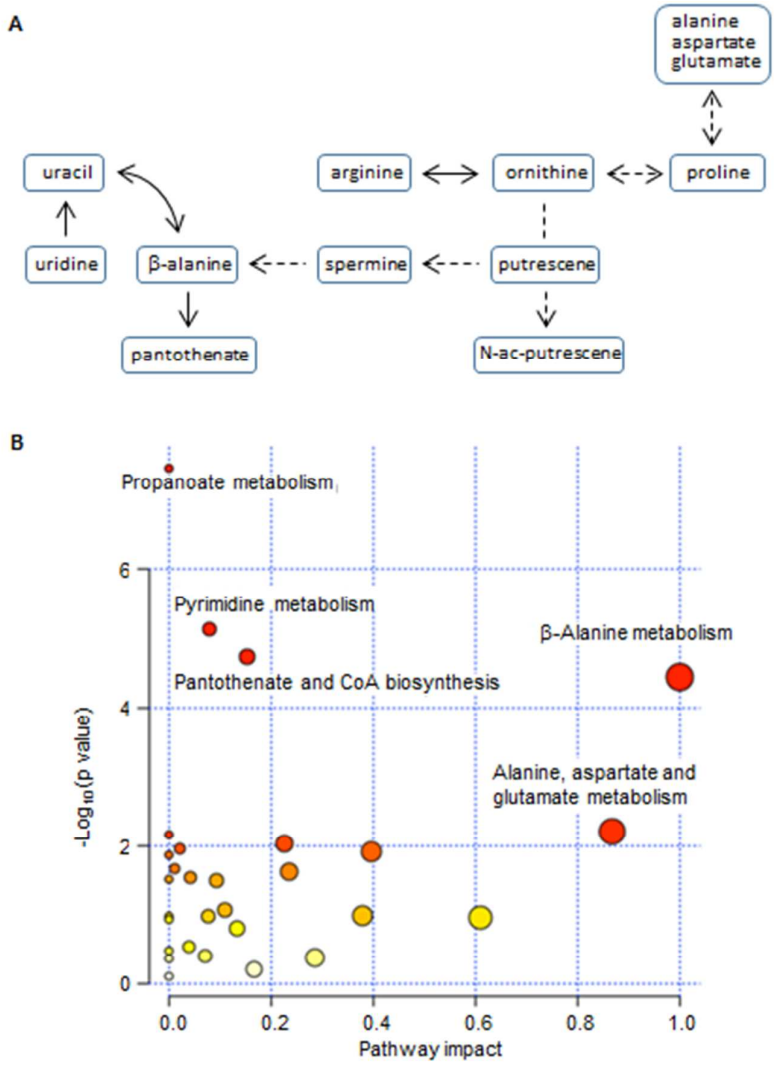

For TOC only

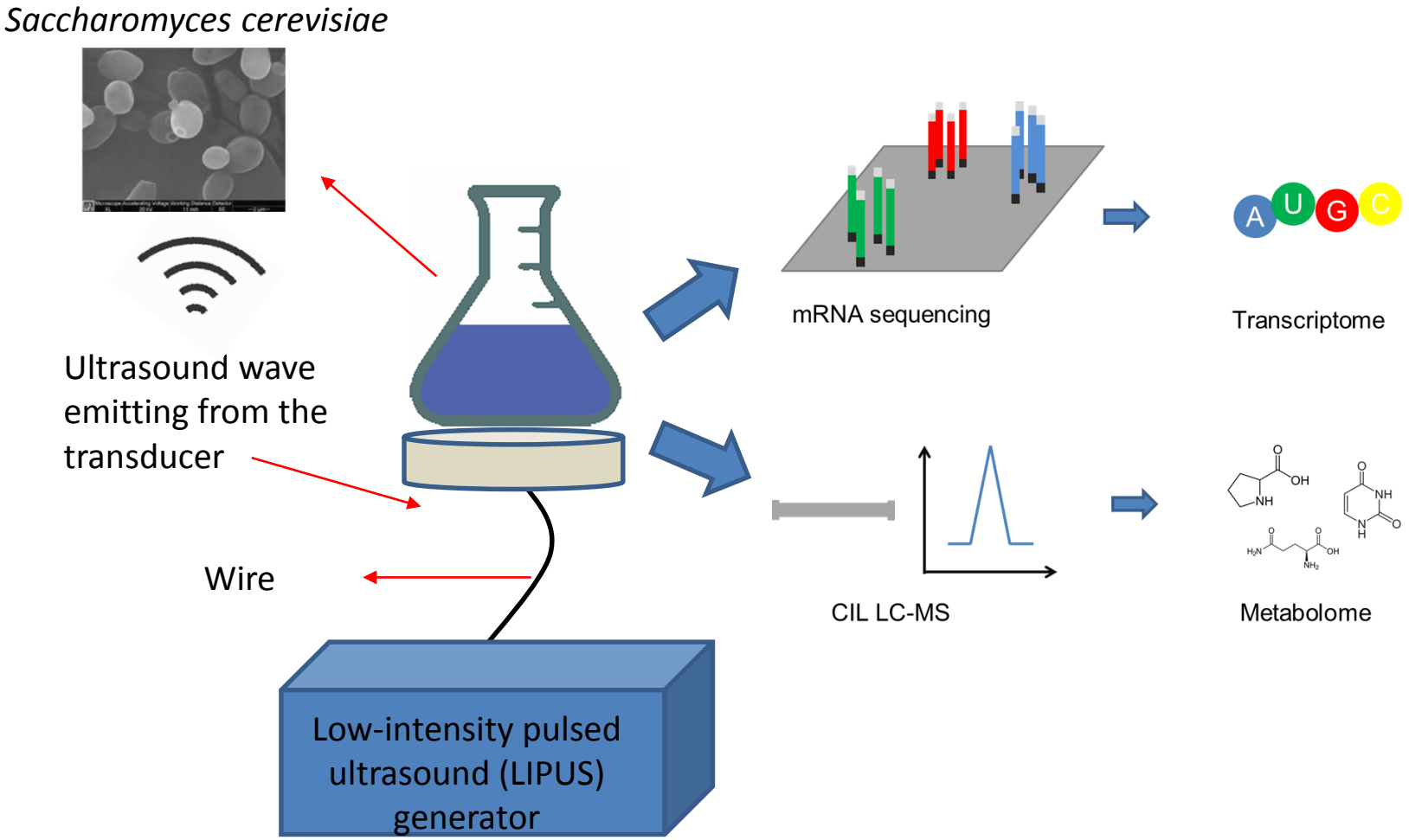
Saccharomyces cerevisiae
Ultrasound wave emitting from the transducer
Wire
Low-intensity pulsed ultrasound (LIPUS) generator
mRNA sequencing
Transcriptome
A U G C
CIL LC-MS
Metabolome